Comparison of a Neutral Density Model With the SET HASDM Density Database

Daniel R. Weimer[1,2], W. Kent Tobiska[3], Piyush M. Mehta[4], R. J. Licata[4], Douglas P. Drob[5]

[1]Center for Space Science and Engineering Research, Virginia Tech, Blacksburg, Virginia, USA
[2]National Institute of Aerospace, Hampton, Virginia, USA
[3]Space Environment Technologies, Los Angeles, California, USA
[4]Department of Mechanical and Aerospace Engineering, Statler College of Engineering and Mineral Resources, West Virginia University, Morgantown, WV, USA
[5]Space Science Division, U.S. Naval Research Laboratory, Washington, District of Columbia, USA

Key Points:

- Thermosphere neutral densities from the EXTEMPLAR model are compared with the SET HASDM density database for a 20 year time period
- The use of density totals on spherical shells at several altitudes is an effective way to compare the models
- The EXTEMPLAR model performs well at altitudes of 400 km and above where geomagnetic storms produce the largest changes in neutral density

Corresponding author: Daniel Weimer, dweimer@vt.edu

Abstract

The EXospheric TEMeratures on a PoLyhedrAl gRid (EXTEMPLAR) method predicts the neutral densities in the thermosphere. The performance of this model has been evaluated through a comparison with the Air Force High Accuracy Satellite Drag Model (HASDM). The Space Environment Technologies (SET) HASDM database that was used for this test spans the 20 years 2000 through 2019, containing densities at 3 hour time intervals at 25 km altitude steps, and a spatial resolution of 10 degrees latitude by 15 degrees longitude. The upgraded EXTEMPLAR that was tested uses the newer Naval Research Laboratory MSIS 2.0 model to convert global exospheric temperature values to neutral density as a function of altitude. The revision also incorporated time delays that varied as a function of location, between the total Poynting flux in the polar regions and the exospheric temperature response. The density values from both models were integrated on spherical shells at altitudes ranging from 200 to 800 km. These sums were compared as a function of time. The results show an excellent agreement at temporal scales ranging from hours to years. The EXTEMPLAR model performs best at altitudes of 400 km and above, where geomagnetic storms produce the largest relative changes in neutral density. In addition to providing an effective method to compare models that have very different spatial resolutions, the use of density totals at various altitudes presents a useful illustration of how the thermosphere behaves at different altitudes, on time scales ranging from hours to complete solar cycles.

Plain Language Summary

A recently developed computer model predicts the density of the upper atmosphere, in the region known as the thermosphere. Changes in this density following geomagnetic storms can perturb the orbits of the many satellites in this region, leading to imprecise knowledge of their paths and risk of collisions. This model uses measurements of the solar wind and the embedded magnetic field to predict the level of heating in the upper atmosphere, and the resulting expansion of the atmosphere to higher altitudes. In order to test the capabilities of the new model, its calculations were compared with density values derived by an Air Force data assimilation system based on radar tracking of multiple objects in Earth orbit over a 20-year period. The results of this comparison show an excellent agreement, particularly at the higher altitudes where geomagnetic storms have the greatest influence.

1 Introduction

A major focus of space weather research has been on the topic of the mass density of the neutral atoms and molecules in the thermosphere. As the variations in this density perturb the orbital motion of satellites, there has been considerable effort in being able to predict these variations using both empirical models and numerical simulations (Bruinsma et al., 2018; J. Emmert, 2015).

Recently Weimer et al. (2020) had described a new empirical model that calculated exospheric temperatures, the asymptotic limit that the temperature in the thermosphere reaches at high altitudes (Prölss & Bird, 2004), often abbreviated as either T_{ex} or T_{∞}. The temperature inputs to the model were derived from neutral density measurements from multiple satellites. Data from the Challenging Mini-satellite Payload (CHAMP) (Bruinsma et al., 2004) in the years 2002 through 2009 were used, along with the Gravity Recovery and Climate Experiment (GRACE) satellites (Tapley et al., 2004), from 2003 through 2010. These total mass densities were derived from accelerometer measurements of the orbital drag. Additional density data were from the European Space Agency's Swarm mission (Friis-Christensen et al., 2006), for the time period from 30 Nov 2013 through 2017. Orbital motions obtained from Global Positioning System (GPS) receivers on the spacecraft were used to determine the drag (Astafyeva et al., 2017).

To create the empirical model, the temperature values were sorted into 1620 cells on a geodesic, polyhedral grid. These triangular grid cells have nearly equal areas and their edges have arc lengths of approximately 7°. Multiple linear regression fits were then used to obtain an equation for the exospheric temperature at each cell's specific location, as a function of the input parameters. For convenience, the unique acronym EXTEMPLAR was given to this method, for EXospheric TEMperatures on a PoLyhedrAl gRid. The Naval Research Laboratory Mass Spectrometer and Incoherent Scatter radar Extended (NRLMSISE-00) thermosphere model (Hedin, 1991; Picone et al., 2002) was used to convert the density measurements into the exospheric temperatures values that were used for the model development. Afterwards the "MSIS" model (as commonly known) was used to calculate neutral densities using the exospheric temperatures output from EXTEMPLAR for given locations and input parameters. Comparing such density predictions with the original satellite measurements revealed a very good performance by the combination of the EXTEMPLAR and MSIS models (hereafter referred to as simply EXTEMPLAR, with the MSIS component assumed). As there were on the order of ≈100,000 data points in each grid cell, the regression formulas that used only six input variable and 16 coefficients could not contain a memory of specific time periods or events, so this was considered a valid test of the model. Nevertheless, a validation trial using an independent dataset is valuable.

The Air Force High Accuracy Satellite Drag Model (HASDM) (Storz et al., 2005) assimilates radar tracking of several dozens of calibration satellites to obtain thermospheric neutral densities. HASDM continuously adjusts coefficients in a modified Jacchia-Bowman 2008 (JB2008) model (Bowman et al., 2008; Tobiska et al., 2008) to match the radar measurements. While the Combined Space Operations Center (CSpOC) of the United States Space Force (USSF) (previously part the Air Force) archives the temperature-corrected coefficients that have been applied to the JB2008 atmosphere, these data are not available to the public. Space Environment Technologies (SET) validates the HASDM outputs under contract and produces a recreation of the densities of the global atmosphere, calling it the "SET HASDM density database" (Tobiska et al., 2021). With approval of the USSF, SET has released the density values for scientific use. These data span two solar cycles, from January 1, 2000 through December 31, 2019. As stated by Tobiska et al. (2021), "all solar cycle, geomagnetic storm and sub-storm, extended solar flare, and thermospheric cooling perturbations are embedded in the data. Because of its accuracy, time resolution, global scale, and information content, the SET HASDM database densities are suitable for use as a new space weather benchmark for atmospheric expansion against which space weather events are measured." The purpose of this paper is to present the results of a comparison between the EXTEMPLAR and HASDM density values. The comparison was run for the entire, 20-year time period. In addition to serving as a useful validation tool, the results have provided helpful insights into the behavior of the thermosphere over the two solar cycles.

2 Recent EXTEMPLAR Modifications

Work is presently under way to improve the EXTEMPLAR method and develop a real-time, operational program, so the version used in this comparison is similar to but not exactly identical to what was described by Weimer et al. (2020). One difference is that the we now use the newer NRLMSIS 2.0 model (J. T. Emmert et al., 2020) rather than NRLMSISE-00 to calculate the neutral density from the exospheric temperatures.

This change will enable use of future updates to the model. It was found that for the same values of exospheric temperature the densities from the NRLMSISE-00 version were generally 2% greater than from the NRLMSIS 2.0 version at 400 km altitude. These lower density values are actually in better agreement with the CHAMP density dataset provided by Mehta et al. (2017), which had been increased by 2% by Weimer et al. (2016) and Weimer et al. (2020) in their calculations. For the development of the most recent version of EXTEMPLAR, all of the exospheric temperature values were recalculated from the original density measurements (Mehta et al., 2017) using NRLMSIS 2.0. The EXTEMPLAR model that was used in this comparison with the HASDM data is referred to as Version 2.4.2, since is a second-generation model, using the fourth (of several) iterations that were tested, and using version 2 of the NRLMSIS model.

The previous work by Weimer et al. (2020) originally had an objective to determine whether or not measurements of emissions from nitric oxide could be used in predictions of thermospheric temperatures and density. Six formulas or versions of the EXTEMPLAR calculations were reported. As nitric oxide emission measurements are not presently available in real time, the most recent EXTEMPLAR model is most closely related to the previous Version 6, that used only solar indices and Poynting flux values from an empirical model (Weimer, 2005a, 2005b) that can use historical or real-time solar wind and Interplanetary Magnetic Field (IMF) measurements.

As before, the exospheric temperatures are calculated separately for each of 1620 grid cells; this grid is obtained from a 20-facet icosahedron, in which each facet is subdivided into 81 equilateral triangles, with the new vertices projected outward to a sphere. A new feature is that the Poynting flux values are delayed in time, with different time delays used for each grid cell. The result is that when the auroral heating suddenly increases the temperatures in the grid cells near the pole will increase sooner than at locations near the equator, that have a delayed response. Details about these delays will be reported in a separate publication.

The exospheric temperature in each grid cell is obtained from this formula:

$$\begin{aligned} T_{\infty_N} = \; & C_0 + C_1 S_{10} + C_2 S_{10} \sin(\theta_D) + C_3 S_{10} \cos(\theta_D) + \\ & C_4 \sqrt{M_{10}} + C_5 \sqrt{M_{10}} \sin(\theta_D) + C_6 \sqrt{M_{10}} \cos(\theta_D) + \\ & C_7 \sin(2\theta_D) + C_8 \cos(2\theta_D) + C_9 \sin(\phi_{UT}) + C_{10} \cos(\phi_{UT}) + \\ & C_{11} S_T(\delta t_N) \sin(\phi_{UT}) + C_{12} S_T(\delta t_N) \cos(\phi_{UT}) + C_{13} S_T(\delta t_N) + \\ & C_{14} \Delta T \sin(\theta_D) + C_{15} \Delta T \cos(\theta_D) + C_{16} \Delta T \end{aligned} \tag{1}$$

T_{∞_N} is the exospheric temperature in cell number N. S_{10} and M_{10} are solar proxy indices that were developed for use in the JB2008 density model (Tobiska et al., 2008; Thayer et al., 2021). Predictions of these indices are produced by SET, with updated values provided in near real-time. θ_D is calculated using $2\pi DOY/365.25$, which is the Day-Of-Year date converted to radians, and $\phi_{UT} = 2\pi UT/24$ is the Universal Time (UT) converted to radians. The C_7 and C_8 terms reproduce semi-annual/inter-annual variations in the data. $S_T(\delta t_N)$ represents Poynting flux values that have been delayed in time by an amount that is unique for each grid cell N. Sums of the Poynting flux are actually calculated for both the Northern and Southern Hemispheres. As described by Weimer et al. (2020), these totals are combined with a formula that varies smoothly from one hemisphere to the other:

$$S_T = S_N \sin^2(0.5 * (Latitude + \pi/2)) + S_S \sin^2(0.5 * (Latitude - \pi/2)) \tag{2}$$

where S_N and S_N are the total Poynting flux values in the Northern and Southern hemispheres respectively. The latitude is determined from the geometric center of each grid cell's geometric center. In radians, this latitude ranges from $-\pi/2$ to $+\pi/2$. The Poynting flux values in this version are smoothed with a boxcar averaging function having a width of 1 hr, prior to the application of the time delays, that range from 39 min in polar regions to 6.6 hr at low latitudes.

The ΔT in (1) represent a global perturbation to the exospheric temperature, that varies in each grid cell in proportion to C_{14}, C_{15}, and C_{16}. ΔT varies in time, as calculated with the following numerical difference equation:

$$\Delta T(t_{n+1}) = \Delta T(t_n) - \Delta T(t_n) \left(\frac{\delta t}{\tau_c} \right) + \alpha S_T(t_n) - P_{NO}(t_n) \tag{3}$$

In each time step ΔT increases in proportion (α) to the total Poynting flux in both hemispheres (S_T), and decays at an exponential rate with time constant τ_c. ΔT is further decreased by the radiative, cooling power of nitric oxide emissions, represented by P_{NO}.

This power is simulated with use of difference equations, using exactly the same methods described by Weimer et al. (2020) in equations (10) and (11). As in the previous versions of the model, the various parameters in the difference equations were optimized through reiterative fits of the T_{∞_N} from (1) with the temperature values in each cell.

3 Density Calculations Using NRLMSIS 2.0

It is helpful to review how the MSIS model is used with the EXTEMPLAR program in order to obtain the neutral densities. This description helps with understanding some some of the results that will be shown. The standard input parameters for MSIS are the geographic coordinates, altitude, date, time, solar $F_{10.7}$ index (both daily and 81-day average), and the daily A_p index of geomagnetic activity. There is an option to include values of the ap index over six, 3-hour intervals. To obtain the neutral densities

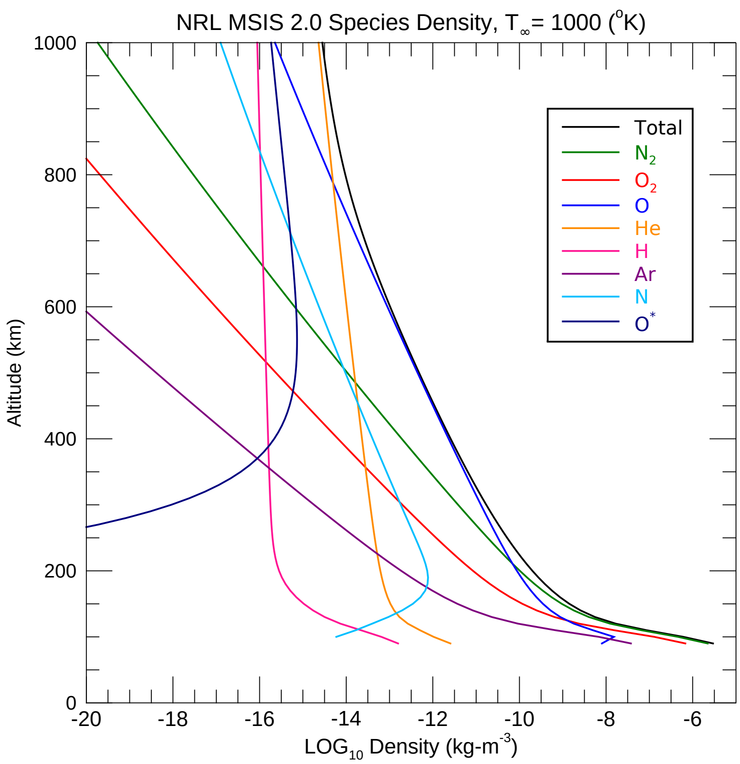

Figure 1. Example of densities from NRLMSIS 2.0 as a function of altitude. All species that are calculated are shown, using colors indicated in the legend. Total density shown in black. Input values were 80° latitude, 0 longitude, on Spring equinox at 0 Universal Time. $F_{10.7}$ index was 120 sfu, and A_p index zero, with exospheric temperature set to 1000°K.

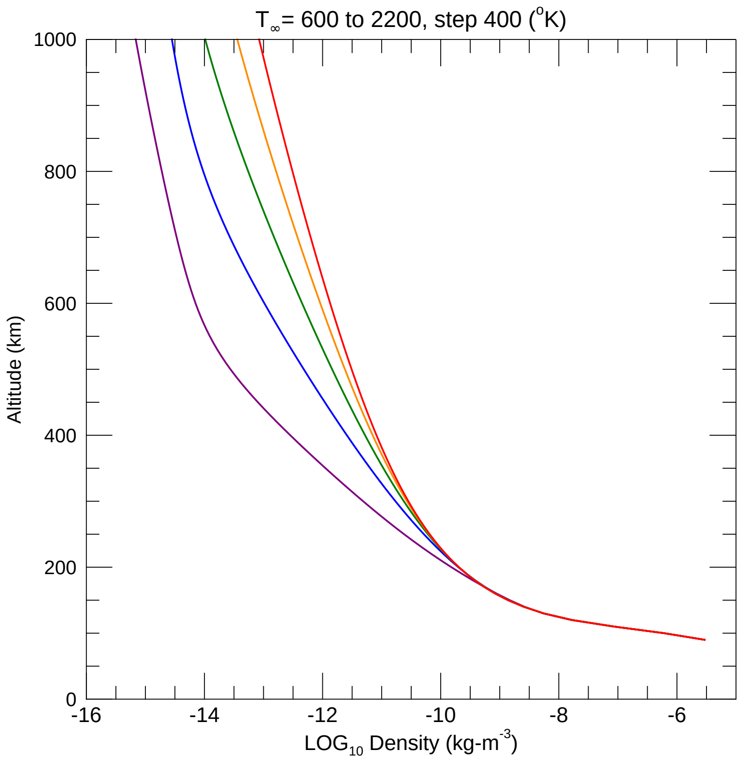

Figure 2. Example of total densities from NRLMSIS 2.0 as a function of altitude, for different values of exospheric temperature. The five lines show results with the exospheric temperature set to 600°, 1000°, 1400°, 1800°, and 2200°K, using the colors purple, blue, green, orange, and red, respectively. Other input parameters are the same as in Figure 1.

in the thermosphere, NRLMSIS 2.0 calculates the density of each atomic and molecular species at a boundary at 122.5 km altitude, along with the temperature and temperature gradient. Normally, MSIS also calculates the exospheric temperature for the given conditions and coordinates. The boundary conditions and exospheric temperature are then used to compute the density of each species as a function of altitude, as illustrated in the example in Figure 1. The species densities are summed to obtain the total density (the black line in the figure).

One shortcoming to the MSIS model is that the actual values of the A_p index are obtained only after measurements from magnetometers at selected, global locations are processed. So real-time indices are not available. While there are predictions of A_p available, they are only estimates. As geomagnetic indices are only an indirect proxy for the amount of heating that occurs in the polar regions, it is assumed that a model of the Poynting flux should be more accurate. Furthermore, as the solar wind velocity and IMF values are the primary input needed to obtain the Poynting flux, values can be obtain from real-time measurements having an approximately 1 hr lead time, rather than much later. That is one reason why the use of exospheric temperatures from the EXTEMPLAR model is advantageous. It also uses the solar indices S_{10} and M_{10}, that are considered to be more accurate than $F_{10.7}$ alone since they represent the actual solar irradiance being deposited into the thermosphere (Bowman et al., 2008; Tobiska et al., 2008).

With a small modification to the MSIS program, the exospheric temperature that is calculated by the EXTEMPLAR model is included as a new input parameter. This temperature (if included) replaces the value that MSIS calculates internally. Figure 2 illustrates the effect of changing the exospheric temperature in MSIS, with densities as a function of altitude shown for temperatures of 600, 1000, 1400, 1800, and 2200°K. Note that at an altitude of 200 km, the exospheric temperature variations have little effect on the total density.

4 Comparison with HASDM

The complete SET HASDM density database is available at `https://spacewx.com/hasdm/`. As indicated by Tobiska et al. (2021), this data "covers the period from January 1, 2000 through December 31, 2019. Data records exist every 3 h during solar cycles 23 and 24. The database has a grid size of $10° \times 15°$ (latitude, longitude) with 25 km altitude steps between 175 and 825 km." One difficulty is that the resolution of this grid is much more coarse than the approximately 4° spanned by the sides of the 1620, triangular cells in the EXTEMPLAR model. As the HASDM model, and the JB2008 model from which it was derived, use spherical harmonics having low order and degree, using smaller grid spacings for the HASDM data archive would not have helped much to improve the resolution of details.

For purpose of comparison, the HASDM grid values were interpolated to the centers of the geodesic grid cells used in EXTEMPLAR. An example of such a comparison is shown in Figure 3, from 26 October, 2003 at 6 h Universal Time (UT). In this example (and others not shown) it is apparent that the EXTEMPLAR densities have features that do not appear in the HASDM map. On the other hand, comparisons of EXTEMPLAR densities with CHAMP and GRACE measurements had indicated that small-scale variations in the density variations do exist (Weimer et al., 2020). Reports on complex, localized density enhancements had previously been reported on numerous occasions (Schlegel et al., 2005; Sutton et al., 2005; Bruinsma et al., 2006; Crowley et al., 2010).

It was decided that the best way to compare the results from models having different resolutions is to calculate the total density integrated over the surface of a sphere at a given altitude, and compare these totals. The totals are obtained by taking the density value in each grid cell and multiplying it by the area of that cell at the selected radius, and then summing these products. In the case of the HASDM database, the interpolated values are used. As the grid areas were precomputed in units of square radians, they only needed to be multiplied by the radius squared, in units of m^2. Since the densities have units of kg/m^3, these integrated sums have units of kg/m. In the example in Figure 3, the totals are indicated above each map in the upper-right corners. These sums were computed for every 3 hr interval in the SET HASDM density database, for

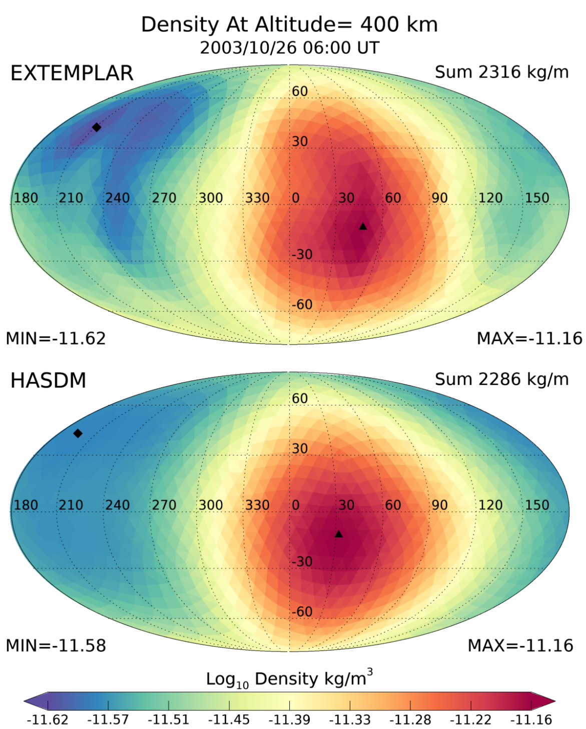

Figure 3. Example of neutral densities from EXTEMPLAR (top) and HASDM (bottom), mapped at 400 km altitude. Values are calculated for 26 October, 2003, at 6 h UT. Results from integrating over the surface of a sphere at 400 km altitude are indicated in the upper right corners.

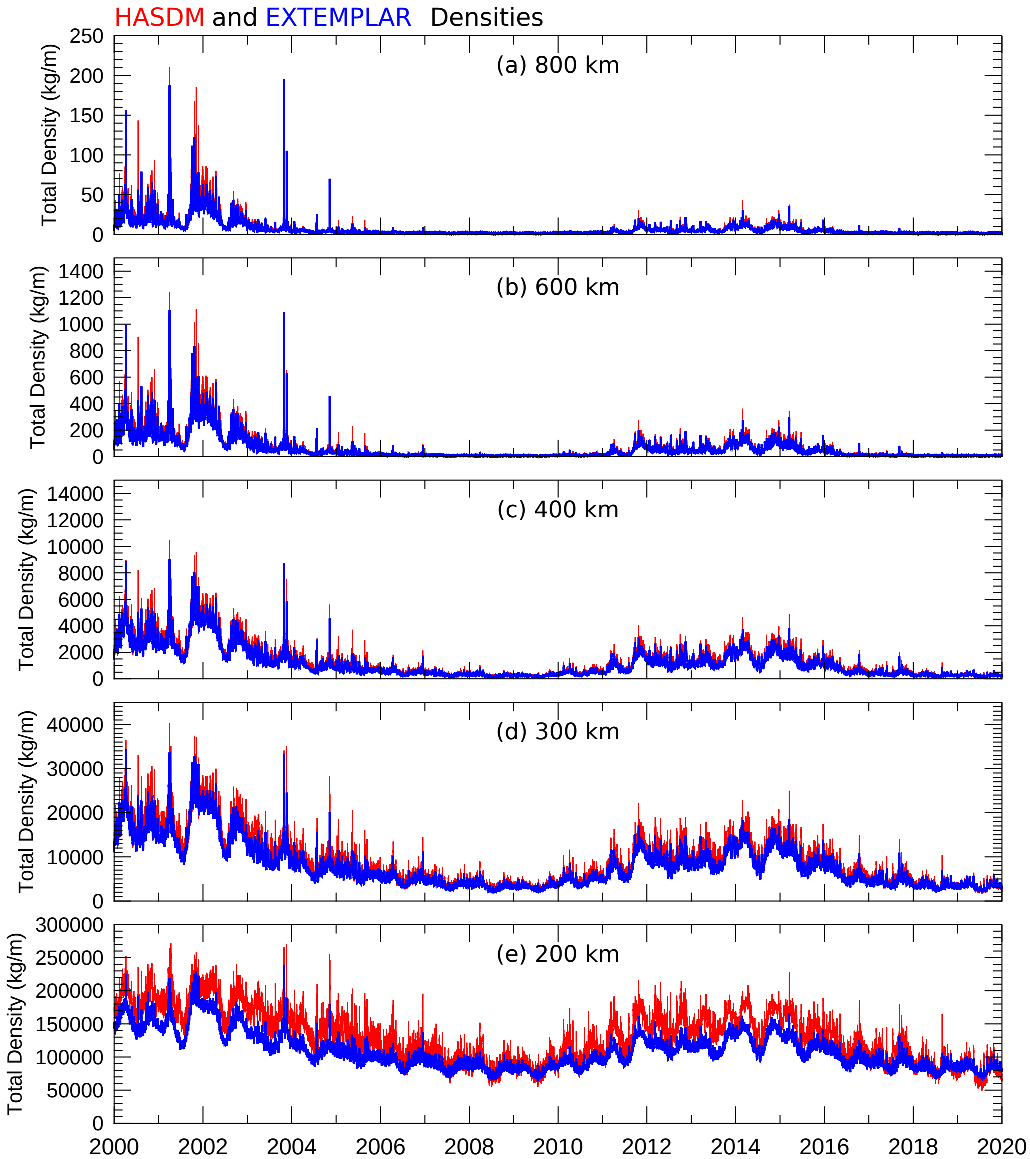

Figure 4. Integrated densities graphed as a function of time, for the time period from 1 January, 2000 through 31 December, 2019. HASDM results are shown in red and EXTEMPLAR in blue, for altitudes of 800, 600, 400, 300, and 200 km (top to bottom).

the entire 20-year time period, at altitudes of 200, 300, 400, 600, and 800 km. The results are shown as a function of time in Figure 4. Solar wind velocity and IMF values measured by the Advanced Composition Explorer (ACE) spacecraft during this time period were input to the Poynting flux model used in the EXTEMPLAR program.

Obviously, the two models are in excellent agreement at most altitudes, although HASDM often has slightly larger values. The differences are largest at 200 km. While both models track the same trends over time, the HASDM values at this altitude tend to be larger than from EXTEMPLAR. However, as illustrated in Figure 2, at 200 km altitude the variations in the exospheric temperature have little influence on the density at this altitude; the density values at this altitude are determined entirely by the conditions calculated within the MSIS 2.0 model.

A closer look at the time period spanning years 2001 through 2004 is shown in Figure 5, for altitudes 800, 600, 400, and 300 km, from top to bottom. An expanded look at the active time period in late 2003 is presented in Figure 6, covering the time period from 16 October through 24 November 2003, containing two extreme geomagnetic storms. Figure 7 contains another interesting time period, from 1 July 2004 through 30 November 2004. The first event within this time has three, successive peaks in the neutral density, followed by an event in November having two larger density peaks in succession. Additional details can be seen in the Supporting Information document that contains 20 separate plots for each of the years in the SET HASDM density database.

5 Correlations and Standard Deviations

Linear correlation coefficients of the two time series were calculated for each year, with the results shown in Figure 8(a). The blue, red, green, brown, and black lines represent altitudes of 200, 300, 400, 600, and 800 km, respectively. In general, the correlations hover around 0.95 for altitudes of 300 to 600 km, while the correlation for 200 km altitude tends to range from only 0.85 to 0.90. The correlation at 800 km is more variable, being in the high range in some years, but decreasing in years associated with lower solar activity.

Standard deviations are shown in Figure 8(b), using the same line coloring at each altitude. Dividing the deviations by the mean of the HASDM density in each year results in the deviation expressed as a percentage, shown in 8(c). With the exception of the deviations at 800 km before 2005, these percentage errors mostly fall in the range of 10% to 20%.

For comparison, Figure 9 contains estimates of the HASDM errors, that were produced by B. Bowman and provided by Tobiska et al. (2021) in a supplement at `https://`

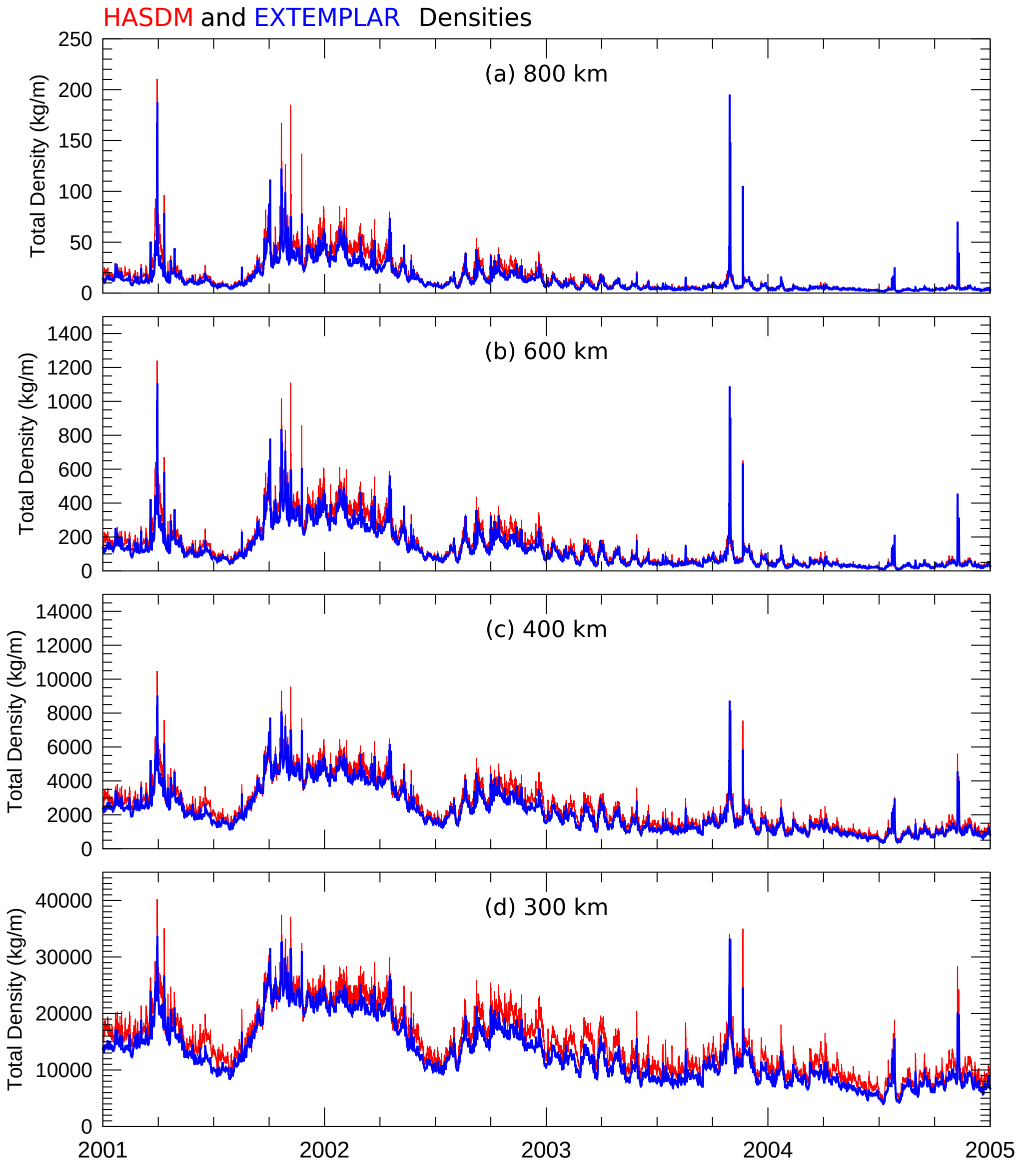

Figure 5. Integrated densities graphed as a function of time, for the time period from 1 January, 2001 through 31 December, 2004. HASDM results are shown in red and EXTEMPLAR in blue, for altitudes of 800, 600, 400, and 300km (top to bottom).

`spacewx.com/hasdm/`. These errors are derived within HASDM by a process known as the Dynamic Calibration Atmosphere (DCA) (Storz et al., 2005). The dots in Figure 8 show the HASDM error for each of the calibration satellites. The HASDM errors tend to range between 2% and 6% during the peaks in the solar cycle (e.g., Figures 8(a) and 8(c)) and increasing to 4% to 10% when solar activity is low (e.g., Figures 8(b) and 8(d)). These uncertainties were obtained by comparing the derived HASDM data assimilated

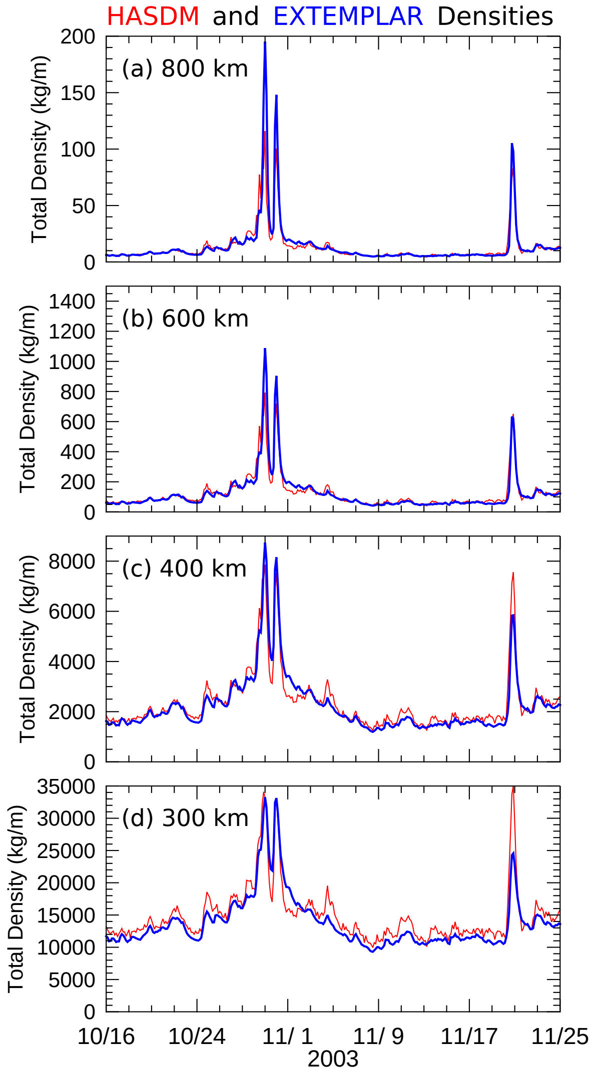

Figure 6. Integrated densities graphed as a function of time, for the time period from from 16 October through 24 November 2003. HASDM results are shown in red and EXTEMPLAR in blue, for altitudes of 800, 600, 400, and 300km (top to bottom).

densities with sets of densities derived from segmented tracking orbit fits to calibration satellites. It is seen in these graphs that the errors are largest at 750 km altitude and above.

6 Discussion

The method in which the neutral densities from different models were integrated over the surface of a sphere at a given altitude has proven to be an effective way to make

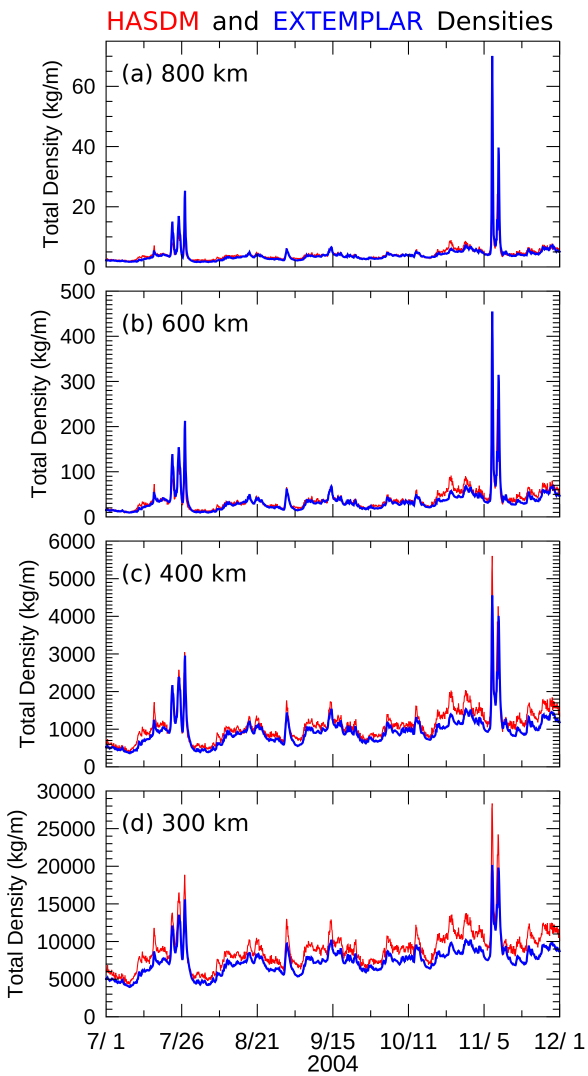

Figure 7. Integrated densities graphed as a function of time, for the time period from from 1 July 2004 through 30 November 2004. HASDM results are shown in red and EXTEMPLAR in blue, for altitudes of 800, 600, 400, and 300 km (top to bottom).

comparisons. The results show a very good agreement between the EXTEMPLAR and HASDM models on scales ranging from years down to hours. The correlations between the two models at the smallest scales, as seen in Figures 6 and 7 is excellent. The EXTEMPLAR predictions match the HASDM values especially well during the most extreme events, most notably at 400 km altitude and above.

The results are helpful for illustrating how the thermosphere behaves over time at different altitudes, including the annual and solar cycle variability in addition to dur-

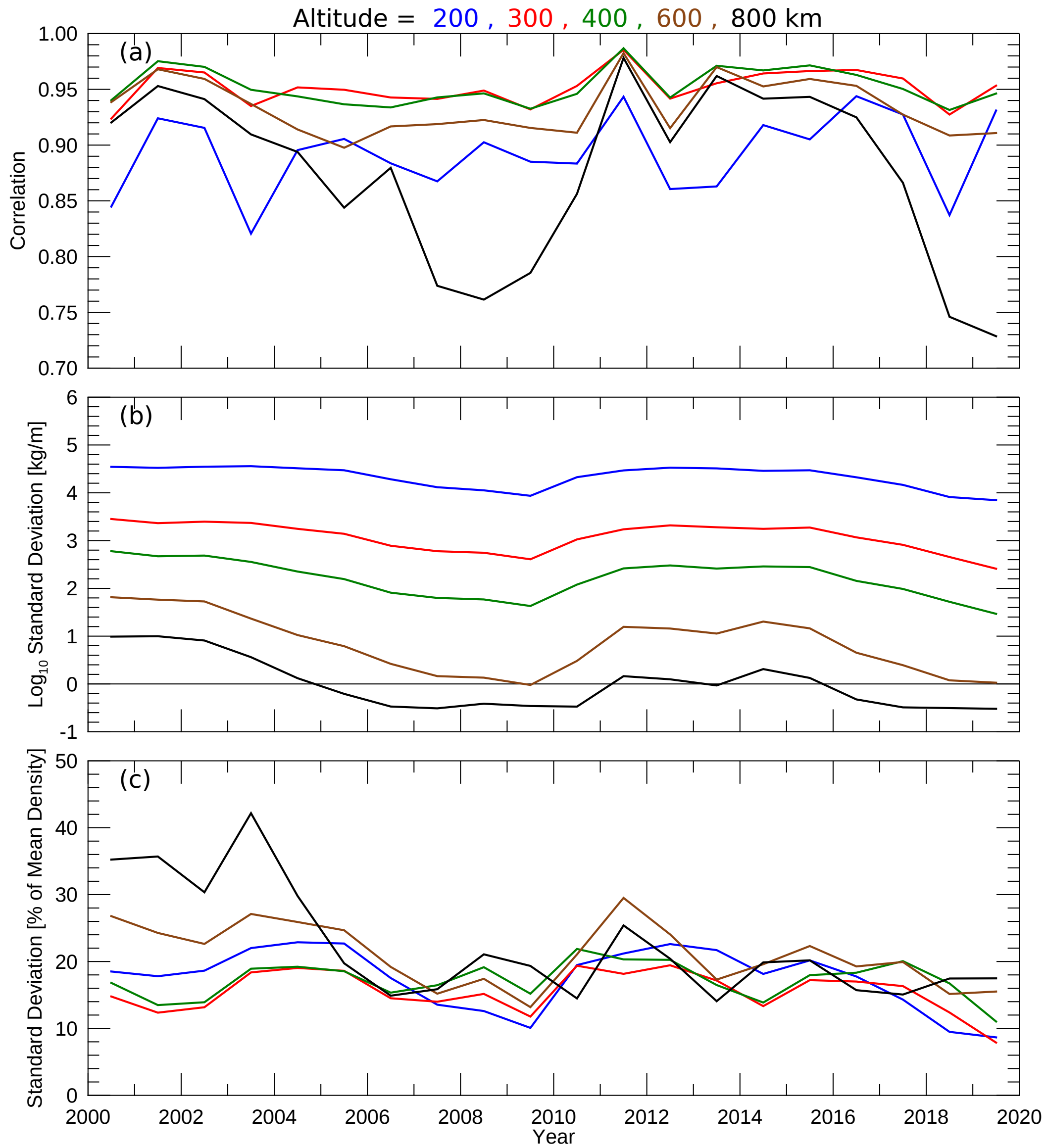

Figure 8. Correlations and Standard Deviations. (a) HASDM and EXTEMPLAR correlation coefficients for all years. The blue, red, green, brown, and black lines represent altitudes of 200, 300, 400, 600, and 800 km, respectively. (b) Standard deviations, in units of kg/m, using the same line colors. (c) Standard deviations expressed as a percentage of the mean density in each year.

ing major events. It is seen that geomagnetic storms have the greatest influence at higher altitudes, where there are substantial changes in the neutral density with respect to pre-storm levels.

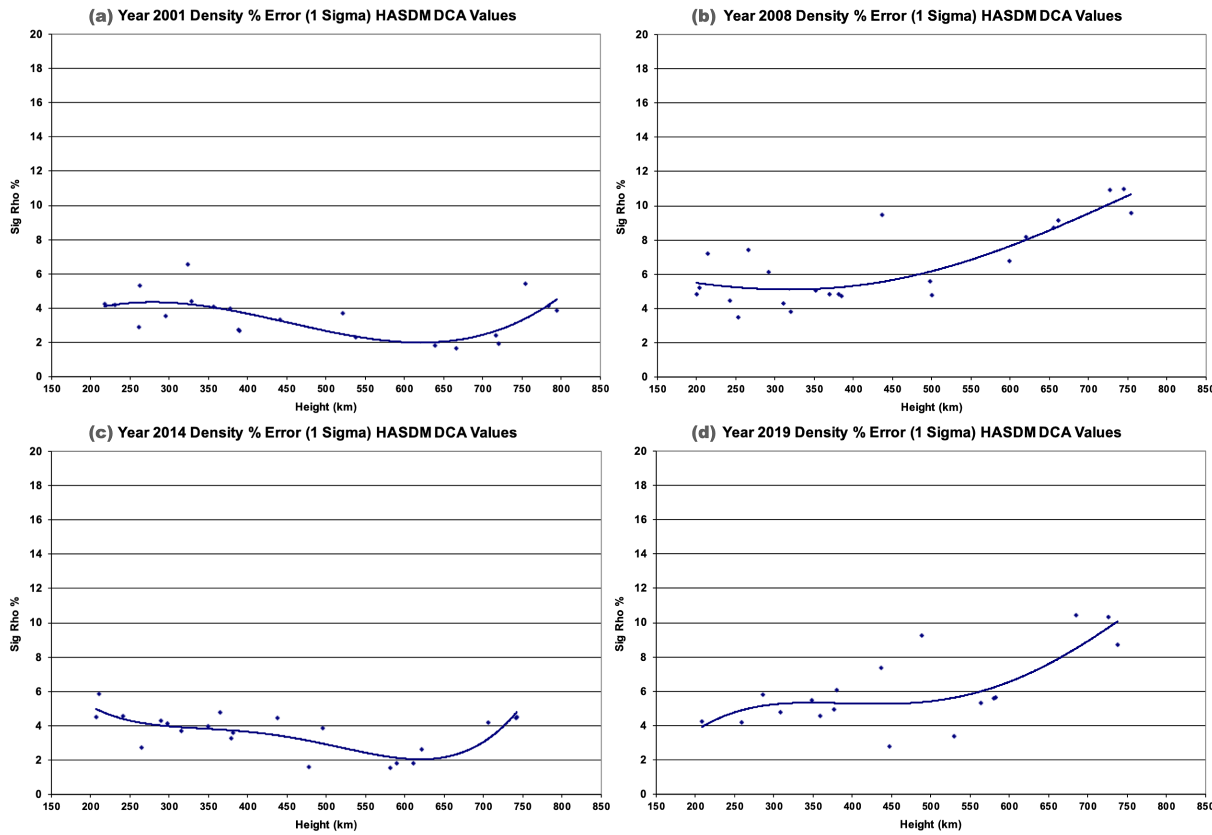

Figure 9. HASDM errors as a function of altitude. The four parts show the errors for the years (a) 2001, (b) 2008, (c) 2014, and (d) 2019.

The correlations graphed in Figure 8(a) between 300–600 km are 0.95, which we consider to be very good. While the correlations at 200 km and 800 km altitude are lower (in the range of 0.85 to 0.90), they are still reasonable. At 200 km altitude the exospheric temperature calculations have little effect on the density variations, as shown in Figure 2. Perhaps the differences could be reduced with some fine tuning of the MSIS 2.0 model, and we are studying this possibility.

Results at 800 km are the most inconsistent. Figure 9 also indicates that the HASDM errors are the largest here, particularly during times of low solar activity, as shown in 9(b) and 9(d). Solar minimum also coincides with the lowest correlations at 800 km (black line in 8(a). The plots in the Supporting Information for the years 2007, 2008, 2009, 2017, 2018, and 2019 show that the HASDM system has a nearly flat line during the early and mid-year time periods when semi-annual variations usually occur, while EXTEMPLAR produced the decreases in the density that are the expected signatures of these semi-annual variations (J. T. Emmert & Picone, 2010).

At 800 km altitude the EXTEMPLAR densities tend to exceed the HASDM values during the large geomagnetic storms, such as in late October in Figure 6(a). This is the cause of the increase in the black line in 2003 in Figure 8(c). It can be argued that the densities calculated by the EXTEMPLAR-MSIS combination could more accurate than HASDM at this altitude, since the sparse atmosphere may have little effect on the segmented orbit density fits.

It was mentioned earlier that HASDM has a coarse spatial resolution, while satellite measurements indicate that the density often varies over distances that are smaller than can be resolved with this model. In cases were the total densities of the two models are in agreement, the EXTEMPLAR-MSIS combination is likely more accurate.

Oftentimes the integrated densities from HASDM are slightly greater than those from EXTEMPLAR. In a comparison between the SET HASDM dataset with the JB2008 model and CHAMP and GRACE density measurements, Licata et al. (2021) had found that the HASDM density values were also consistently greater than the values derived from the CHAMP and GRACE accelerometer measurements, while matching better than the JB2008 model. Licata et al. (2021) also found that during the major storm in October 2003 (the same event shown here in the first half of Figure 6), while the HASDM dataset had slightly larger densities than measured with CHAMP and GRACE, it did very well at matching the relative changes in density during this period.

7 Conclusion

The comparison of the densities calculated by the EXTEMPLAR program with the values in the SET HASDM database show that EXTEMPLAR performs very well. As the HASDM assimilation system relies on radar tracking of multiple satellites to derive the neutral densities, it is expected to be very accurate. But it cannot predict the response of the neutral density to sudden geomagnetic storms in advance, before the tracking measurements can be obtained. On the other hand, the EXTEMPLAR program can use the real-time measurements of the solar wind velocity and IMF to make predictions approximately 1 hr ahead of the thermosphere's response to extreme space weather events. This lead provides time to issue alerts or calculate perturbations to satellite orbits.

The EXTEMPLAR results shown here had used Level 2 science data from the ACE satellite, which had a better quality than the real-time data provided by ACE. Presently the real-time solar wind measurements are provided by the Deep Space Climate Observatory (DSCOVR). The quality of the real-time DSCOVR solar wind and magnetic field measurements are just as good as the ACE Level 2 data, so this change will not degrade the performance of EXTEMPLAR. The solar indices are also updated in near real time by SET.

Other developers of thermosphere models, either empirical or numerical, are encouraged to compare their neutral density calculations with the SET HASDM density database in a similar manner. The total, integrated densities shown in Figure 4 are available in an archive at `https://doi.org/10.5281/zenodo.3xxxxxxx` for the entire, 20 year time period. As mentioned earlier, these data are of value for studying how the neutral density at different altitudes vary on time scales ranging from hours to solar cycles.

Acronyms

ACE Advanced Composition Explorer

CHAMP Challenging Mini-satellite Payload satellite

DCA Dynamic Calibration Atmosphere

DSCOVR Deep Space Climate Observatory

EXTEMPLAR EXospheric TEmperatures on a PoLyhedrAl gRid

GRACE Gravity Recovery and Climate Experiment satellite

HASDM High Accuracy Satellite Drag Model

JB2008 Jacchia-Bowman 2008 neutral density model

MSIS Short abbreviation referring to the either of the NRL density models

NRLMSISE-00 Naval Research Laboratory Mass Spectrometer and Incoherent Scatter radar Extended density model 2000

NRLMSIS 2.0 Naval Research Laboratory Mass Spectrometer and Incoherent Scatter radar model, Version 2.0

SET Space Environment Technologies

Data Availability Statement

A data archive containing the integrated neutral densities on spherical shells at altitudes of 200, 300, 400, 600, and 800 km, from both EXTEMPLAR and HASDM, is available at `https://doi.org/10.5281/zenodo.5177065`. The Supporting Information document contains graphs of these integrated densities for each of the 20 years. The original SET-HASDM database access and supplementary information can be found at `https://spacewx.com/hasdm/`. The ACE level 2 data are available from the NASA archives at `ftp://cdaweb.gsfc.nasa.gov/pub/data/ace`. The solar indices are available from Space Environment Technologies at `http://sol.spacenvironment.net/JB2008/indices`.

(The reserved Zenodo DOI link noted above will become active only after this paper is accepted. A temporary copy of this archive is now at: `https://bit.ly/2X79AZ4`**)**

Acknowledgments

Daniel Weimer was supported by NASA grant 80NSSC20K1362 to Virginia Tech, through the Space Weather Operations-to-Research Program. Kent Tobiska, Piyush Mehta, and Richard Licata were supported by subcontracts to Space Environment Technologies and West Virginia University. Douglas Drob was supported by NASA interagency agreement 80HQTR20T0081 with the Naval Research Laboratory. Daniel Weimer had additional support from NSF grant AGS-2019465.

References

Astafyeva, E., Zakharenkova, I., Huba, J. D., Doornbos, E., & van den IJssel, J. (2017). Global ionospheric and thermospheric effects of the june 2015 geomagnetic disturbances: Multi-instrumental observations and modeling. *J. Geophys. Res.: Space Physics*, *112*, 11,716–11,742. doi: 10.1002/2017JA024174

Bowman, B. R., Tobiska, W. K., Marcos, F. A., Huang, C. Y., Lin, C. S., & Burke, W. J. (2008). A new empirical thermospheric density model JB2008 using new solar and geomagnetic indices. In *AIAA/AAS astrodynamics specialist conference proceedings.* Honolulu, HI.

Bruinsma, S., Forbes, J. M., Nerem, R. S., & Zhang, X. (2006). Thermosphere density response to the 20–21 november 2003 solar and geomagnetic storm from CHAMP and GRACE accelerometer data. *J. Geophys. Res.*, *111*. doi: 10.1029/2005JA011284

Bruinsma, S., Sutton, E., Solomon, S. C., Fuller-Rowell, T., & Fedrizzi, M. (2018). Space weather modeling capabilities assessment: Neutral density for orbit determination at low earth orbit. *Space Weather*, *16*(11), 1806–1816. doi: 10.1029/2018SW002027

Bruinsma, S., Tamagnan, D., & Biancale, R. (2004). Atmospheric densities derived from CHAMP/STAR accelerometer observations. *Planet. Space Sci.*, *52*, 297.

Crowley, G., Knipp, D. J., Drake, K. A., Lei, J., Sutton, E., & Lühr, H. (2010). Thermospheric density enhancements in the dayside cusp region during strong b_y conditions. *Geophys. Res. Lett.*, *37*. doi: 10.1029/2009GL042143

Emmert, J. (2015). Thermospheric mass density: A review. *Advances in Space Research*, *56*(5), 773 - 824. Retrieved from `http://www.sciencedirect.com/science/article/pii/S0273117715003944` doi: http://dx.doi.org/10.1016/j.asr.2015.05.038

Emmert, J. T., Drob, D. P., Picone, J. M., Siskind, D. E., Jones Jr, M., Mlynczak, M. G., … Yuan, T. (2020). NRLMSIS 2.0: A whole-atmosphere empirical model of temperature and neutral species densities. *Earth and Space Science*, *7*, e2020EA001321. Retrieved from `https://agupubs.onlinelibrary.wiley.com/doi/abs/10.1029/2020EA001321` doi: 10.1029/2020EA001321

Emmert, J. T., & Picone, J. M. (2010). Climatology of globally averaged thermospheric mass density. *J. Geophys. Res.*, *115*(A09326). doi: 10.1029/2010JA015298

Friis-Christensen, E., Lühr, H., & Hulot, G. (2006). Swarm: A constellation to study the Earth's magnetic field. *Earth, Planets and Space*, *58*(4), 351–358. doi: 10.1186/BF03351933

Hedin, A. E. (1991). Extension of the MSIS thermosphere model into the middle and lower atmosphere. *J. Geophys. Res.*, *96*, 1159–1172.

Licata, R. J., Mehta, P. M., Tobiska, W. K., Bowman, B. R., & Pilinski, M. D. (2021). Qualitative and quantitative assessment of the SET HASDM database. *Space Weather*, *n/a*(n/a), e2021SW002798. Retrieved from `https://agupubs.onlinelibrary.wiley.com/doi/abs/10.1029/2021SW002798` doi: https://doi.org/10.1029/2021SW002798

Mehta, P. M., Walker, A. C., Sutton, E. K., & Godinez, H. C. (2017). New density estimates derived using accelerometers on board the champ and grace satellites. *Space Weather*, *15*(4), 558–576. (2016SW001562) doi: 10.1002/2016SW001562

Picone, J., Hedin, A., Drob, D., & Aikin, A. (2002). NRLMSISE-00 empirical model of the atmosphere: Statistical comparisons and scientific issues. *J. Geophys. Res.*, *107*(A12). doi: 10.1029/2002JA009430

Prölss, G. W., & Bird, M. K. (2004). *Physics of the earth's space environment: an introduction*. Springer-Verlag Berlin Heidelberg. (ISBN 3-540-21426-7)

Schlegel, K., Lühr, H., St.-Maurice, J.-P., Crowley, G., & Hackert, C. (2005). Thermospheric density structures over the polar regions observed with CHAMP. *Ann. Geophys.*, *23*, 1659–1672.

Storz, M. F., Bowman, B. R., Branson, M. J. I., J.Casali, S., & Tobiska, W. K. (2005). High accuracy satellite drag model (HASDM). *Advances in Space Research*, *36*(12), 2497–2505. doi: https://doi.org/10.1016/j.asr.2004.02.020

Sutton, E. K., Forbes, J. M., & Nerem, R. S. (2005). Global thermospheric neutral density and wind response to the severe 2003 geomagnetic storms from CHAMP accelerometer data. *J. Geophys. Res.*, *110*. doi: 10.1029/2004JA010985

Tapley, B. D., Watkins, S. B. M., & Reigber, C. (2004). The gravity recovery and climate experiment: Mission overview and early results. *Geophys. Res. Lett*, *31*. doi: 10.1029/2004GL019929

Thayer, J. P., Tobiska, W. K., Pilinski, M. D., & Sutton, E. K. (2021). Remaining issues in upper atmosphere satellite drag. In *Space weather effects and applications* (pp. 111–140). American Geophysical Union (AGU). Retrieved from `https://agupubs.onlinelibrary.wiley.com/doi/abs/10.1002/9781119815570.ch5` doi: https://doi.org/10.1002/9781119815570.ch5

Tobiska, W. K., Bouwer, S. D., & Bowman, B. R. (2008). The development of new solar indices for use in thermospheric density modeling. *J. Atmos. Sol. Terr. Phys.*, *70*, 803–819.

Tobiska, W. K., Bowman, B. R., Bouwer, S. D., Cruz, A., Wahl, K., Pilinski, M. D., ... Licata, R. J. (2021). The SET HASDM density database. *Space Weather*, *19*(4), e2020SW002682. Retrieved from `https://`

agupubs.onlinelibrary.wiley.com/doi/abs/10.1029/2020SW002682 doi: https://doi.org/10.1029/2020SW002682

Weimer, D. R. (2005a). Improved ionospheric electrodynamic models and application to calculating Joule heating rates. *J. Geophys. Res.*, *110*. doi: 10.1029/2004JA010884

Weimer, D. R. (2005b). Predicting surface geomagnetic variations using ionospheric electrodynamic models. *J. Geophys. Res.*, *110*. doi: 10.1029/2005JA011270

Weimer, D. R., Mehta, P. M., Tobiska, W. K., Doornbos, E., Mlynczak, M. G., Drob, D. P., & Emmert, J. T. (2020). Improving neutral density predictions using exospheric temperatures calculated on a geodesic, polyhedral grid. *Space Weather*, *18*(1), e2019SW002355. doi: 10.1029/2019SW002355

Weimer, D. R., Sutton, E. K., Mlynczak, M. G., & Hunt, L. A. (2016). Intercalibration of neutral density measurements for mapping the thermosphere. *J. Geophys. Res.*, *121*, 5975–5990. doi: 10.1002/2016JA022691